Optics and Lasers in Engineering 96 (2017) 117–123

Contents lists available at ScienceDirect

Optics and Lasers in Engineering

journal homepage: www.elsevier.com/locate/optlaseng

Microscopic structured light 3D profilometry: Binary defocusing technique vs. sinusoidal fringe projection

Beiwen Li, Song Zhang *

School of Mechanical Engineering, Purdue University, West Lafayette, IN 47907, USA

ARTICLE INFO

Article history:
Received 13 April 2016
Received in revised form
27 May 2016
Accepted 8 June 2016
Available online 20 June 2016

Keywords:
High-speed
High-resolution
Microscopic
Binary defocusing
Telecentric lens

ABSTRACT

This paper compares the binary defocusing technique with conventional sinusoidal fringe projection under two different 3D microscopic profilometry systems: (1) both camera and projector use telecentric lenses and (2) only camera uses a telecentric lens. Our simulation and experiments found that the binary defocusing technique is superior to the traditional sinusoidal fringe projection method by improving the measurement resolution approximately 19%. Finally, by taking the speed advantage of the binary defocusing technique, we presented a high-speed (500 Hz) and high-resolution (1600 × 1200) 3D microscopic profilometry system that could reach kHz.

1. Introduction

In recent years, 3D optical metrology has shown great prospect in the field of manufacturing in applications such as inspection and rapid prototyping. The structured light (SL) system has obtained increasing popularity among existing 3D shape measurement technologies owing to its flexibility, speed and accuracy [1]. For the real implementation of such technology in the field of industrial metrology, one of the main challenges is to boost its measurement accuracy up to microscale level.

To transport SL 3D profilometry into microscale level, researchers first attempted to modify the optics of a regular SL system. A variety of approaches have shown their successes for microscopic SL 3D profilometry, such as inserting digital-micro-mirror-device (DMD), liquid-crystal-display (LCD) or liquid-crystal-on-silicon (LCoS) chips into one channel of a stereo microscope [2–7]. Through this approach, Van der Jeught et al. [7] have realized 120 Hz microscopic 3D profilometry in real-time by utilizing the graphics processing unit (GPU) for real-time 3D data processing and visualization, which is similar to what have been realized in macro-scale measurement systems [8–10]. There are also research works that change the lenses into non-telecentric lenses with small field-of-view (FOV) and long working distance (LWD) [11–15]. Lately, telecentric lenses are utilized as an alternative to those non-telecentric methods owing to their larger depth of focus (DOF) [16–19]. These aforementioned approaches have successfully overcome the hardware limitations of SL 3D profilometry and boosted the measurement accuracy into the level of tens of μm.

Apart from the hardware setups, here we are looking for other possible solutions to enhance the capabilities of 3D microscopic profilometry. One of the possible direction is by examining the effects of different projection patterns. Traditionally, sinusoidal patterns are used for SL 3D profilometry, but has some major drawbacks such as nonlinear gamma calibration requirement and speed bottleneck. Since sinusoidal method requires the projection of 8-bit sinusoidal patterns, the measurement speed is limited at the hardware level of the DLP projection devices, even for those lower level developmental kits such as DLP Lightcrafters or Wintech PRO 4500. For instance, in the real-time microscopic 3D profilometry system developed by Van der Jeught et al. [7], phase-shifted sinusoidal patterns are used for structured light illumination, yet the measurement speed is limited at the maximum refreshing rate (i.e. 120 Hz) of 8-bit grayscale patterns for the projector used in their system (i.e. LightCrafter 3000). Lei and Zhang [20] proposed the binary defocusing method which feeds the projector with 1-bit binary pattern, and then projects quasi-sinusoidal patterns through projector defocusing. Since only two grayscale values are used, the binary defocusing method does not require gamma calibration. With the advanced digital-light-processing (DLP) technology, it has also reached the measurement speeds up to kHz. For instance, the same DLP LightCrafter 3000 used in [7] can refresh 1-bit binary patterns up to 4000 Hz.

Since the binary pattern provides the highest possible contrast,

* Corresponding author.
E-mail address: szhang15@purdue.edu (S. Zhang).

http://dx.doi.org/10.1016/j.optlaseng.2016.06.009
0143-8166/

we hypothesize that the binary defocusing method can also increase signal to noise ratio (SNR) of the digital fringe projection (DFP) system and thus improve measurement accuracy. In this research, we developed two different types of microscopic SL system with DLP projectors to test our hypothesis. The first system uses a telecentric lens for the camera, and an LWD pinhole lens for the projector; the second system uses telecentric lenses for both the camera and the projector. We then compared the measurement resolutions of the binary defocusing method with traditional sinusoidal method under both systems. Both simulations and experimental results demonstrated that in a microscopic SL system with a DLP projector, the binary defocusing technology can improve measurement resolution approximately 19% over the traditional sinusoidal method. Moreover, with the high refreshing rate of 1-bit patterns using the DMD, it has enabled the high-speed and high-resolution 3D microscopic profilometry capabilities. For example, we have developed a high-speed (500 Hz) and high-resolution (1600×1200) 3D microscopic profilometry system that could potentially reach kilohertz (kHz) frame rates.

Section 2 introduces the theoretical background involved in this research, including phase-shifting algorithms, binary defocusing technology and the principles of our two different microscopic SL profilometry systems. Section 3 demonstrates the simulations which compare binary defocusing and traditional sinusoidal methods with the existence of noise. Section 4 shows the experimental validations and Section 5 summarizes this paper.

2. Principle

In this section, we will introduce the related principles of each technology used in this research, which includes the least-squares phase-shifting algorithm, the binary defocusing technique, as well as the models of the two types of microscopic SL systems that we built.

2.1. Least-squares phase-shifting algorithm

Phase-shifting algorithms are frequently implemented in optical metrology because of their flexibility and accuracy. In a generalized least-square phase-shifting algorithm, the i-th projected fringe can be mathematically formulated as

$$I_i(x, y) = I'(x, y) + I''(x, y)\cos(\phi + 2i\pi/N), \tag{1}$$

where $I'(x, y)$ represents the average intensity, $I''(x, y)$ denotes the intensity modulation, and $\phi(x, y)$ is the phase to be solved for. Generally speaking, the more phase-shifting steps used, the better the phase quality that can be obtained:

$$\phi(x, y) = -\tan^{-1}\left[\frac{\sum_{i=1}^{N} I_i \sin(2i\pi/N)}{\sum_{i=1}^{N} I_i \cos(2i\pi/N)}\right]. \tag{2}$$

This equation generates the wrapped phase ranging $(-\pi, \pi]$. We adopted a simple binary coding method [21] to retrieve an absolute phase map without 2π discontinuities. The phase information can be converted into 3D geometry using a simple reference-plane-based calibration method [22].

2.2. Binary defocusing technique

The basic principle of binary defocusing technique [20] can be explained as follows: different from traditional sinusoidal method, it feeds the projector with 1-bit square binary patterns. If the projector is properly defocused, a quasi-sinusoidal fringe pattern can be projected on the screen. The theoretical background of binary defocusing technique lies in suppressing the higher order harmonics of a square wave in Fourier series expansion. Since the projector defocusing can be approximated by a low-pass Gaussian blurring effect, therefore it is possible to suppress higher order harmonics of a square wave through projector defocusing, and thus making the first order harmonic (sinusoidal) to be dominant in the resultant pattern.

According to Ekstrand and Zhang [23], if a nine-step phase-shifting algorithm is applied, it is possible to perform high quality measurements even with nearly focused binary patterns. Nine-step phase-shifting approach can effectively reduce error caused by projector nonlinearity for sinusoidal pattern projection and high order harmonics due to binary patterns, and also suppress random noise from the camera. The use of nearly focused projector instead of perfectly focused projector is (1) to increase the contrast of the fringe images, or SNR and (2) to remove the discrete pixel effect of digital projectors. Therefore, to examine the performance of binary defocusing method in microscale 3D profilometry, and meanwhile compare it with traditional sinusoidal method, we applied nine-step phase-shifting ($N=9$) algorithm under both approaches with a nearly focused projector for fair comparison.

2.3. Microscopic structured light 3D profilometry systems

In this research, we built two different types of microscopic SL system. The first system is called *single-telecentric SL system*, which uses a telecentric lens for the camera and a pinhole lens for the projector. The second system is called *dual-telecentric SL system*, which uses telecentric lenses for both the camera and the projector.

The model of this *single-telecentric SL system* is illustrated in Fig. 1(a). In this system, the projector uses an LWD pinhole lens, which respects the well-known pinhole model. The camera in this system uses telecentric lens, which respects an orthographic projection model. The lens simply produces a linear magnification along X and Y axes, meaning it is not sensitive to the depth variation along Z-axis.

The telecentric lens has the unique properties of orthographic projection, low distortion, magnification constancy and larger DOF [24], and thus is more preferable in microscopic measurement. In this research, we also built a *dual-telecentric SL system*, as illustrated in Fig. 1(b), in which both the camera and the projector use telecentric lenses.

3. Simulations

To compare the binary defocusing technique with traditional sinusoidal method in terms of noise reduction, we did some simulations which compare the performance of the two methods when Gaussian noise presents. In the simulation, nine-step ($N=9$) phase shifted patterns are used. As discussed in Section 2.2, using nine-step ($N=9$) phase-shifting algorithm reduces random noise caused by camera, as well as the nonlinearity caused by projector for sinusoidal fringe pattern projection or high frequency harmonics caused by binary pattern projection. The Gaussian noise is used to emulate the camera noise effect in real experiments. We first compared the two methods under one specific Gaussian noise level. The generated phase shifted patterns are "polluted" by a zero-mean Gaussian noise with a standard deviation of 0.05 in intensity. It is important to note that to emulate a nearly focused scenario, we did not add any Gaussian filter to the generated patterns. We computed the phase map using both methods with the algorithm described in Section 2.1, and the resultant phase maps are shown in Fig. 2(a) and (b). We then took a cross section from both phase maps and evaluated the phase errors by

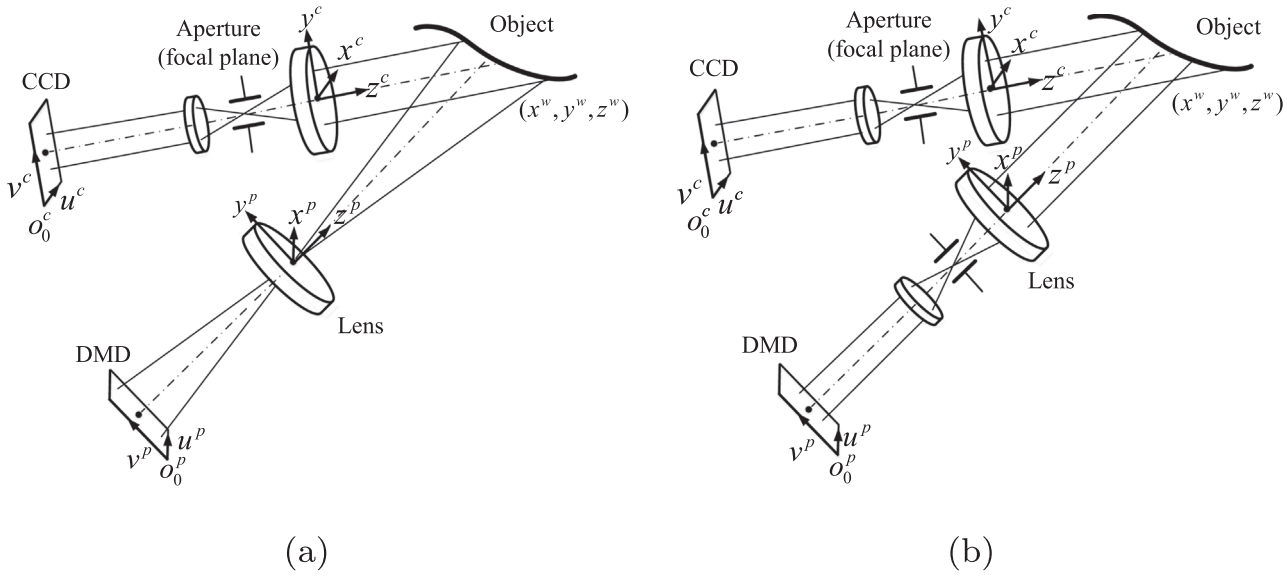

Fig. 1. Schematic diagram of 3D microscopic profilometry systems. (a) *Single-telecentric SL system* and (b) *dual-telecentric SL system*.

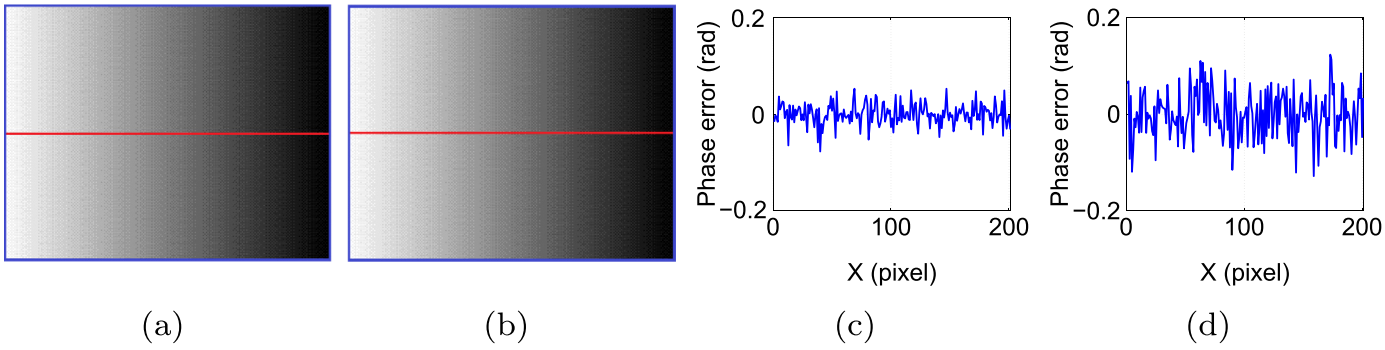

Fig. 2. Comparison between binary defocusing technique and traditional sinusoidal method under Gaussian noise with $\sigma = 0.05$. (a) Phase obtained from binary pattern; (b) phase obtained from sinusoidal pattern; (c) a cross section of phase error from (a) with an RMS error of 0.023 rad; and (d) a cross section of phase error from (b) with an RMS error of 0.047 rad.

removing their gross slopes. The phase error plots are shown in Fig. 2(c) and (d). The corresponding root-mean-square (RMS) errors of the two methods are 0.023 rad and 0.047 rad respectively, which indicates that the phase error of sinusoidal method is almost twice as big as the error of binary defocusing method. Therefore, it clearly depicts that binary defocusing method outperforms the sinusoidal method under this noise level.

To carry out a more thorough evaluation, we also compared the two approaches under different noise levels using image averaging technology. Namely, each of the nine-step phase shifted pattern $I_i(x, y)$ is generated by an average of L same corresponding patterns "polluted" by the same level of Gaussian noise:

$$I_i(x, y) = \frac{1}{L}\left[\sum_{t=1}^{L} I_{it}(x, y) \otimes W_\sigma(x, y)\right], \tag{3}$$

where $W_\sigma(x, y)$ denotes the time-varying Gaussian white noise with zero-mean and a standard deviation σ. Here, we still keep the same $\sigma = 0.05$ all the time. Owing to the randomness of the noise, as L increases, the effect of time varying random noise will be significantly reduced by image averaging. We then compared the two approaches from no image averaging to $L=40$ image averaging to simulate different noise levels. The comparison result is shown in Fig. 3, from which we can see that the phase error from binary defocusing method is always smaller than sinusoidal method. When there is no image averaging, i.e. the noise level is the highest, their difference is the biggest. As the number L of

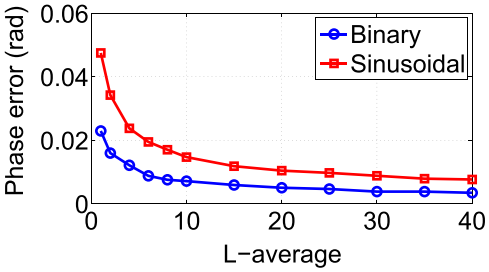

Fig. 3. Comparison between binary defocusing technique and traditional sinusoidal method with different number L of image averaging.

averaging increases, i.e. the noise level decreases, their difference becomes less significant, but binary defocusing method still outperforms sinusoidal method. It clearly illustrates that the binary defocusing method is more resistant to the camera noise than sinusoidal method, which could be explained by its higher image contrast. In next section, we will validate this hypothesis with experimental analysis.

4. Experiments

The *single-telecentric SL system* includes a DLP projector (Model: Wintech Pro 4500) and a digital CCD camera (Imaging

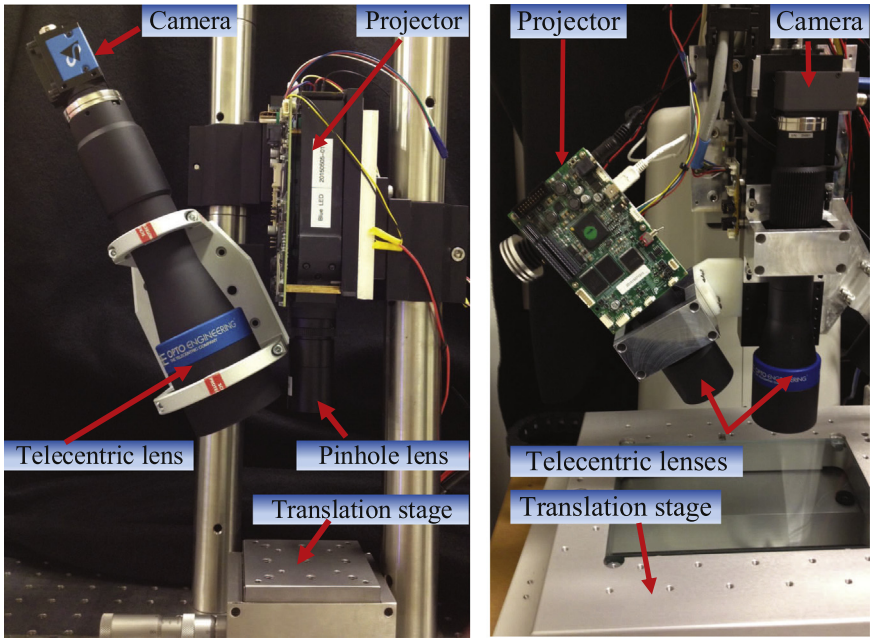

Fig. 4. Picture of the actual test systems. (a) *Single-telecentric SL system* and (b) *dual-telecentric SL system*.

Source DMK 23U274). The projector can refresh 8-bit grayscale patterns at 120 Hz and 1-bit binary patterns at 4225 Hz. The projector resolution is 912 × 1140 with a pixel size of 7.6 × 7.6 μm^2. The camera has a pixel resolution of 1600 × 1200 with a pixel size of 4.7 × 4.7 μm^2. The model of the telecentric lens used for the camera is Opto-engineering TC4MHR036-C, which has a magnification of 0.487, a working distance of 102.5 mm and a field depth of 5 mm. The projector uses an LWD lens with a working distance of 700 mm. The precision vertical translation stage used in this system is Newport M-MVN80 (sensitivity: 50 nm), which is used to perform reference-plane-based calibration [22]. A snapshot of the actual system is shown in Fig. 4(a).

The *dual-telecentric SL system* uses a DLP lightCrafter 4500 projector and a high-resolution digital CMOS camera (Model: PixelLink PL-D725MU-T). Similarly, the projector can refresh 8-bit grayscale patterns at 120 Hz, and 1-bit binary patterns at 4225 Hz. The projector resolution is 912 × 1140 with a pixel size of 7.6 × 7.6 μm^2. The camera resolution is 2592 × 2048 with a pixel size of 4.8 × 4.8 μm^2. The telecentric lens used for the camera is Opto-Engineering TC4M036-C, which has the same specifications as the one used in the previous system. The customized telecentric lens used for the projection system has a magnification of 0.287. It has a working distance of 100 mm a field depth of 10 mm. The precise translation stage with an *X*–*Y*–*Z* sensitivity of 0.1 μm is provided by MicroVU Vertex 251UC measurement system, which is again used for calibration purpose. A snapshot of the actual system is shown in Fig. 4(b).

To compare the binary defocusing method with sinusoidal method in microscale measurement, we first measured a flat planar surface to emulate the framework of the simulation (see Section 3). In other words, we compared the two approaches with different numbers *L* of image averaging and under both *single-telecentric* and *dual-telecentric* systems. We made the projector to be nearly focused for both sinusoidal and binary pattern projection, and again, nine-step (N=9) phase-shifting is used to suppress unwanted high-frequency harmonics and error caused by projector nonlinearity, and also to reduce random noise of the camera. Fig. 5(a) and (b) respectively show the measurement results obtained from *single-telecentric* and *dual-telecentric* systems. From which we can see that under both systems, the experiment results agree well with the simulation results shown in Fig. 3. Namely, the binary defocusing method consistently outperforms conventional sinusoidal method, and the error differences become smaller as *L* increases. The biggest error differences again happen where there is no averaging involved (L=1), in which the binary defocusing method can reduce the noise level of the sinusoidal method by approximately 19% for *single-telecentric* system and 12% for *dual-telecentric* system. It is worth to note that for both comparisons,

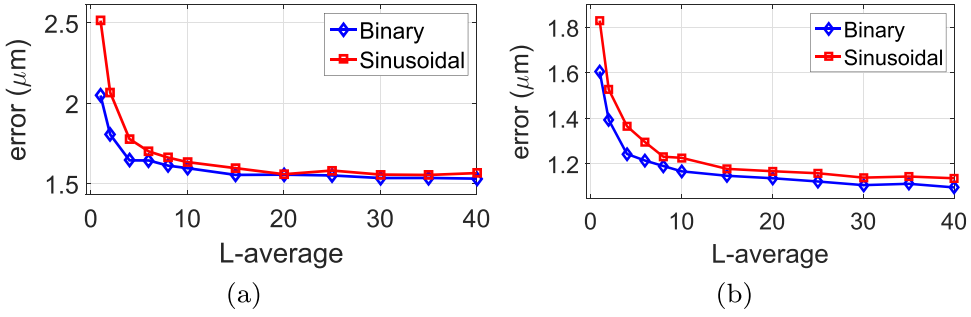

Fig. 5. Flat plane measurement results comparing binary defocusing technique with traditional sinusoidal method using different numbers of image averaging. (a) Using *single-telecentric SL system* and (b) using *dual-telecentric SL system*.

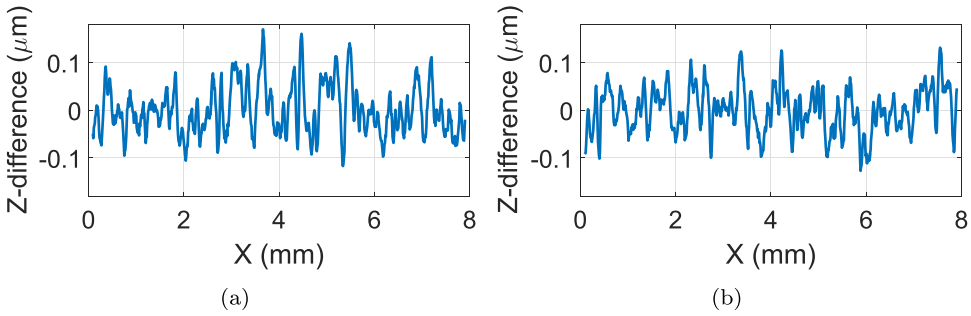

Fig. 6. Difference between binary defocusing and sinusoidal in creating reference plane for (a) *single-telecentric SL system* and (b) *dual-telecentric SL system*. The RMS differences are respectively 0.05 μm and 0.04 μm.

we used sinusoidal patterns to generate reference plane. In particular, we use 18-step ($N=18$) phase-shifted sinusoidal patterns with each fringe being produced by an average of 60 images ($L=60$), and a 9×9 Gaussian filter is then used to further suppress high-frequency random noise. In our experiment, we found that the choice between binary or sinusoidal pattern for reference plane generation does not affect much of the overall noise profile. Fig. 6(a) and (b) shows the differences between generated reference planes from binary and sinusoidal patterns for both systems, from which we can see that under both systems, the differences are very small, with RMS differences of 0.05 μm and 0.04 μm respectively, which only accounts for less than 5% of the overall noise profile. This experiment validates that binary defocusing method has better performance than sinusoidal method in microscale 3D profilometry even if our noise extraction procedure is slightly biased to sinusoidal method.

We also measured an object with complex surface geometry using both the binary defocusing and traditional sinusoidal methods, and under both *single-telecentric* and *dual-telecentric* systems. The 3D geometries were reconstructed using nine-step ($N=9$) phase shifting without image averaging techniques ($L=1$). We then performed noise analysis by subtracting the "relative ground truth" 3D data from the reconstructed 3D geometry. The "relative ground truth" 3D data is obtained from 18-step ($N=18$) phase-shifting and $L=60$ averaging. Note that here we did not apply Gaussian filter for the "relative ground truth" data. This is owing to the fact that for complex surface geometry, smooth filters will cause artifacts around sharp changing edges. Figs. 7 and 8 show the reconstructed 3D results, one cross section of the 3D data and the noise profile of a same ball grid array obtained from both approaches and under both systems. The RMS error for *single-telecentric* system is approximately 3.6 μm for binary defocusing, and 4.1 μm for the sinusoidal method; for the *dual-telecentric* system, the corresponding RMS errors are respectively 2.7 μm and 3.4 μm for the binary defocusing method and for the sinusoidal method. These experiments also indicate that under both systems, the binary defocusing method outperforms the sinusoidal method, which again proved our previous hypothesis.

Finally, we measured a dynamic fluid flow to demonstrate the high-speed 3D microscopic profilometry capabilities of the binary defocusing method. The system was built by replacing the camera in the *single-telecentric SL system* by a high-speed CMOS camera (Vision Research Phantom V9.1). The sample fluid we chose is a small droplet of plain yogurt. In this experiment, we blow the yogurt droplet from one side with a straw, and set both the projection and image capturing speed at 500 Hz, which is not possible for the conventional sinusoidal method with the same hardware setup. The camera resolution we used here is 1600×1200 pixels. In this experiment, we used three phase-shifted binary dithered patterns [25] with a fringe period of $T=45$ pixels to compute wrapped phase, and another three binary dithered patterns with a fringe period of $T=1140$ pixels to perform temporal phase

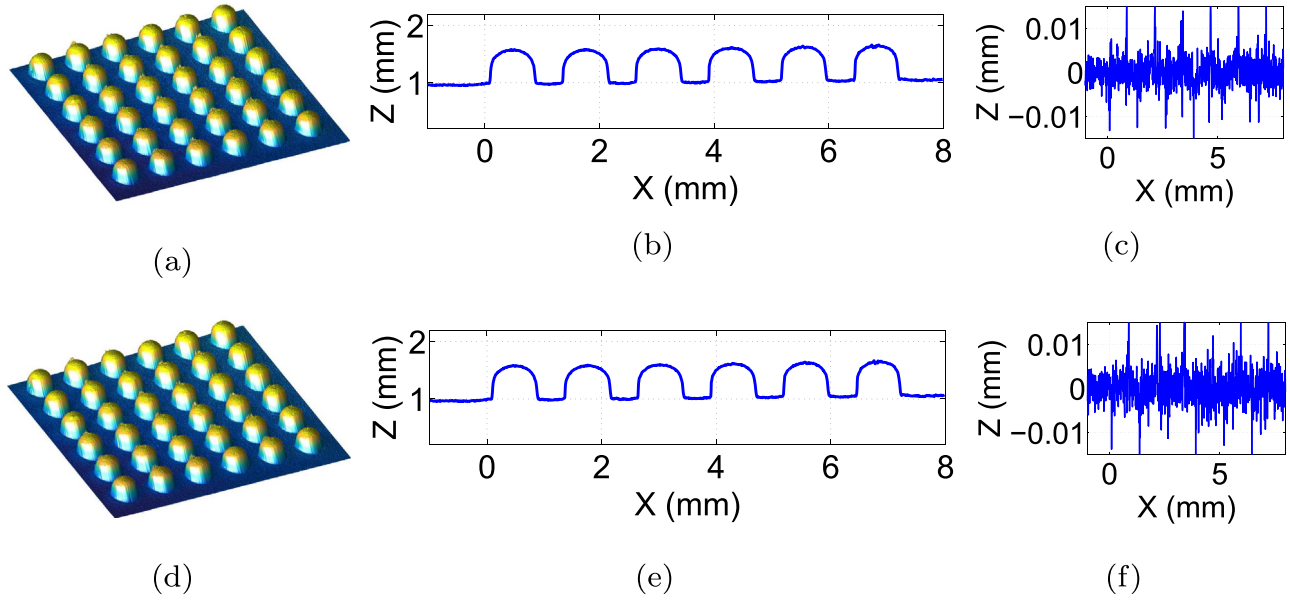

Fig. 7. 3D reconstruction of an object with complex surface geometry using the *single-telecentric SL system*. (a) Reconstructed 3D geometry of the object using binary defocusing method; (b) a cross section of (a); (c) the error plot of (b), the RMS error is 3.6 μm; and (d)–(f) corresponding plots using sinusoidal method, the RMS error is 4.1 μm.

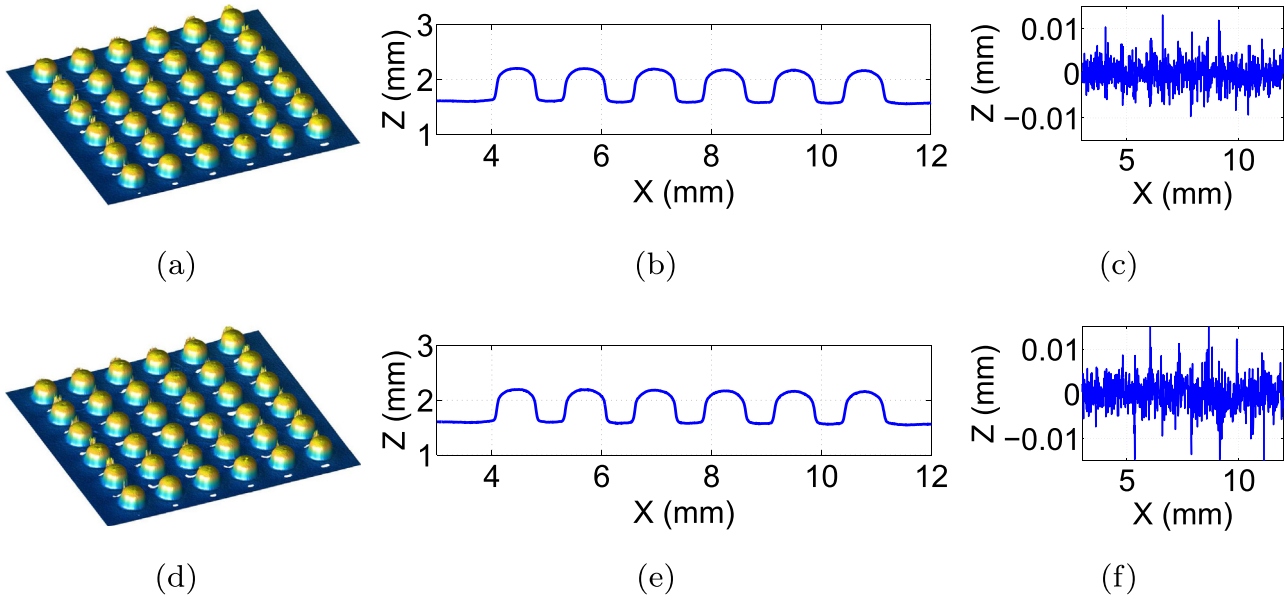

Fig. 8. 3D reconstruction of an object with complex surface geometry using the *dual-telecentric SL system*. (a) Reconstructed 3D geometry of the object using binary defocusing method; (b) a cross section of (a); (c) the error plot of (b), the RMS error is 2.7 μm; and (d)–(f) corresponding plots using sinusoidal method, the RMS error is 3.4 μm.

unwrapping [26]. The unwrapped phase was then used to recover 3D geometry using the calibrated data.

Fig. 9 and its associated videos (Video 1: https://engineering.purdue.edu/ZhangLab/videos/OLE_Li_Video1.mp4 and Video 2: https://engineering.purdue.edu/ZhangLab/videos/OLE_Li_Video2.mp4) demonstrate the measurement results of this dynamic yogurt flow. Fig. 9(a)–(c) illustrates three sample frames of the object texture, whose image contrasts are strengthened a little bit for better visualization purpose. Fig. 9(d)–(f) shows the corresponding 3D profiles. The results indicate that this dynamic fluid flow can be well measured by our 3D microscopic profilometry system. It is worth to note that some vertical creases shown on the 3D geometries are actually produced by the ripples in the flow.

5. Summary

In this research, we compared the binary defocusing technique with traditional sinusoidal method in microscopic SL systems with DLP projectors. Both simulations and experiments demonstrate that the binary defocusing method outperforms the sinusoidal method in 3D microscopic profilometry. The improvement in depth resolution can reach approximately 19%. Finally, by taking the speed advantage of the binary defocusing method, we also

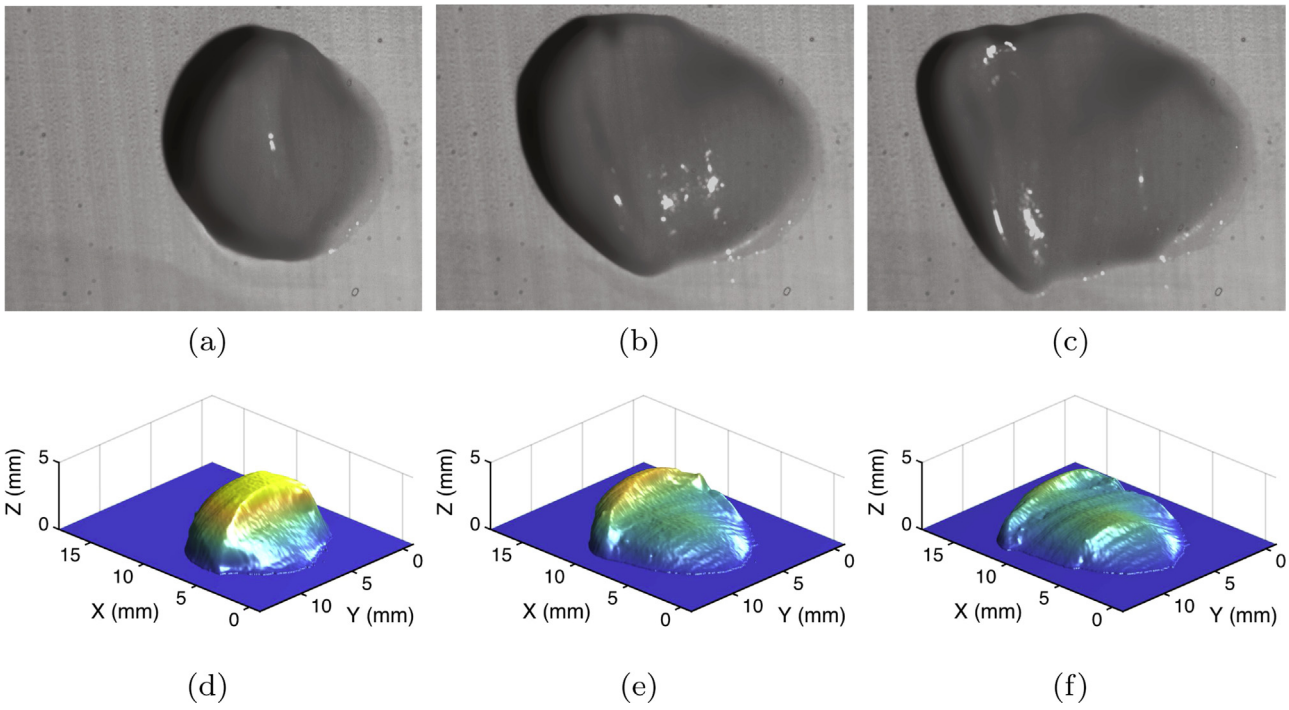

Fig. 9. High-speed 3D microscopic profilometry. (a)–(c) Three sample frames of texture (associated Video 1: https://engineering.purdue.edu/ZhangLab/videos/OLE_Li_Video1.mp4) and (d)–(f) three frames of the 3D geometry (associated Video 2: https://engineering.purdue.edu/ZhangLab/videos/OLE_Li_Video2.mp4).

built a high-speed microscale 3D measurement system to perform 3D microscopic profilometry with the binary defocusing method at a frame rate of 500 Hz.

Acknowledgments

This study was sponsored by the National Science Foundation (NSF) under grant numbers CMMI-1531048. The views expressed in this paper are those of the authors and not necessarily those of the NSF.

References

[1] Gorthi SS, Rastogi P. Fringe projection techniques: whither we are?. Opt Lasers Eng 2010;48:133–40.
[2] Windecker R, Fleischer M, Tiziani HJ. Three-dimensional topometry with stereo microscopes. Opt Eng 1997;36(12):3372–7.
[3] Zhang C, Huang PS, Chiang F-P. Microscopic phase-shifting profilometry based on digital micromirror device technology. Appl Opt 2002;41(28):5896–904.
[4] Proll K-P, Nivet J-M, Körner K, Tiziani HJ. Microscopic three-dimensional topometry with ferroelectric liquid-crystal-on-silicon displays. Appl Opt 2003;42(10):1773–8.
[5] Rodriguez-Vera R, Genovese K, Rayas J, Mendoza-Santoyo F. Vibration analysis at microscale by talbot fringe projection method. Strain 2009;45(3):249–58.
[6] Li A, Peng X, Yin Y, Liu X, Zhao Q, Körner K, et al. Fringe projection based quantitative 3d microscopy. Optik 2013;124(21):5052–6.
[7] Van der Jeught S, Soons JA, Dirckx JJ. Real-time microscopic phase-shifting profilometry. Appl Opt 2015;54(15):4953–9.
[8] Karpinsky N, Hoke M, Chen V, Zhang S. High-resolution, real-time three-dimensional shape measurement on graphics processing unit. Opt Eng 2014;53(2):024105.
[9] Zhang S, Royer D, Yau S-T. GPU-assisted high-resolution, real-time 3-d shape measurement. Opt Express 2006;14(20):9120–9.
[10] Liu K, Wang Y, Lau DL, Hao Q, Hassebrook LG. Dual-frequency pattern scheme for high-speed 3-d shape measurement. Opt Express 2010;18:5229–44.
[11] Quan C, He XY, Wang CF, Tay CJ, Shang HM. Shape measurement of small objects using LCD fringe projection with phase shifting. Opt Commun 2001;189(1):21–9.
[12] Quan C, Tay CJ, He XY, Kang X, Shang HM. Microscopic surface contouring by fringe projection method. Opt Laser Technol 2002;34(7):547–52.
[13] Chen J, Guo T, Wang L, Wu Z, Fu X, Hu X. Microscopic fringe projection system and measuring method. In: Proceedings of the SPIE, Chengdu, China; 2013. p. 87594U.
[14] Mehta DS, Inam M, Prakash J, Biradar A. Liquid-crystal phase-shifting lateral shearing interferometer with improved fringe contrast for 3d surface profilometry. Appl Opt 2013;52(25):6119–25.
[15] Yin Y, Wang M, Gao BZ, Liu X, Peng X. Fringe projection 3d microscopy with the general imaging model. Opt Express 2015;23(5):6846–57.
[16] Zhu F, Liu W, Shi H, He X. Accurate 3d measurement system and calibration for speckle projection method. Opt Lasers Eng 2010;48(11):1132–9.
[17] Li D, Liu C, Tian J. Telecentric 3d profilometry based on phase-shifting fringe projection. Opt Express 2014;22(26):31826–35.
[18] Rao L, Da F, Kong W, Huang H. Flexible calibration method for telecentric fringe projection profilometry systems. Opt Express 2016;24(2):1222–37.
[19] Li B, Zhang S. Flexible calibration method for microscopic structured light system using telecentric lens. Opt Express 2015;23(20):25795–803.
[20] Lei S, Zhang S. Flexible 3-d shape measurement using projector defocusing. Opt Lett 2009;34(20):3080–2.
[21] Zhang S. Flexible 3d shape measurement using projector defocusing: extended measurement range. Opt Lett 2010;35(7):931–3.
[22] Xu Y, Ekstrand L, Dai J, Zhang S. Phase error compensation for three-dimensional shape measurement with projector defocusing. Appl Opt 2011;50(17):2572–81.
[23] Ekstrand L, Zhang S. Three-dimensional profilometry with nearly focused binary phase-shifting algorithms. Opt Lett 2011;35(23):4518–20.
[24] Li D, Tian J. An accurate calibration method for a camera with telecentric lenses. Opt Lasers Eng 2013;51(5):538–41.
[25] Wang Y, Zhang S. Three-dimensional shape measurement with binary dithered patterns. Appl Opt 2012;51(27):6631–6.
[26] Wang Y, Zhang S. Superfast multifrequency phase-shifting technique with optimal pulse width modulation. Opt Express 2011;19(6):5143–8.